AIP | Journal of Applied Physics

Ultrafast heating and resolution of recorded crystalline marks in phase-change media

M. M. Aziz, M. R. Belmont, and C. D. Wright

Citation: J. Appl. Phys. **104**, 104912 (2008); doi: 10.1063/1.3028269
View online: http://dx.doi.org/10.1063/1.3028269
View Table of Contents: http://jap.aip.org/resource/1/JAPIAU/v104/i10
Published by the American Institute of Physics.

Ultrafast heating and resolution of recorded crystalline marks in phase-change media

M. M. Aziz,[a] M. R. Belmont, and C. D. Wright
School of Engineering, Computer Science and Mathematics, University of Exeter, Harrison Building, North Park Road, Exeter EX4 4QF, United Kingdom

(Received 11 April 2008; accepted 9 October 2008; published online 21 November 2008)

This work presents an analytical study of the thermally activated amorphous-to-crystalline phase-change process when the heating source has a delta function temporal profile. This simulates the case of ultrafast heating where crystallization in the amorphous phase-change medium occurs during cooling. The study produced closed-form expressions that predict the necessary peak temperature, and hence energy density, in the phase-change medium for successful crystallization during ultrafast annealing as functions of the kinetic and thermal parameters of the medium. Closed-form expressions were also derived that provide estimates of the final crystalline mark widths and tail lengths when phase change has ceased. The analysis indicated the need to reduce the activation energy of crystallization and the thermal diffusivity of the medium to reduce the initial peak temperature, produced by the heating source, to avoid melting, to increase the crystallization rate, to achieve sufficient levels of crystalline fractions during cooling, and to reduce the size of recorded crystalline marks. Perturbation analysis was carried out to study the effects of latent heat of crystallization during the fast kinetics phase. The result was reductions in the cooling rate of the phase-change material, thus requiring lower peak temperatures to achieve higher volumes of crystalline fraction. Nevertheless, the effects of heat release during crystallization were found to be modest for the class of current phase-change material used in data storage.
 [DOI: 10.1063/1.3028269]

I. INTRODUCTION

Storing information on phase-change media involves heating small volumes of the medium using sources such as lasers or probes to induce phase transformations that result in the production of small amorphous or crystalline marks which have different properties. The amorphous phase is normally characterized by a low reflection coefficient and small electrical conductivity, while the crystalline phase is characterized by higher reflectivity and very large electrical conductivity. The different characteristics of the amorphous and crystalline phases provide the necessary contrast during readback to distinguish between the stored binary states.

The thermally activated phase transition process considered here is complex and the resolution of the final recorded marks is determined by the heat diffusion process and thermal history of the medium in addition to the kinetics of the phase-change process. Much progress has been made, in the form of numerical[1–4] and experimental[2,5–7] studies, to understand the mark formation process, material requirements, and design of thermal layers to support the required recording resolutions and data rates.

To maintain the increases in writing and erasing data rates in storage technologies involving phase-change media, it is equally important to investigate the thermal and kinetic requirements that allow successful crystallization at very high speeds. Although amorphization from the initial crystalline phase has been shown experimentally[8,9] and theoretically[10] to occur within a 1 ns time scale, crystallization has been difficult to achieve in time scales less than hundreds of nanoseconds.[8] Nevertheless, crystallization at shorter time scales has been demonstrated by use of appropriate thermal layers.[9,11]

The present work aims to explore analytic descriptions of the heat flow and the amorphous-to-crystalline phase transition processes during high-speed annealing. This is mainly to study the thermal and kinetic requirements of the phase-change medium (and hence heating source) for successful crystallization during high-speed annealing and to provide estimates of the final widths of recorded crystalline marks and hence resolution of the recording system. The outcomes of the analysis can also contribute toward explaining published experimental observations of high-speed annealing experiments on phase-change media.

The fundamental equations of the heat diffusion process and reaction rate are presented in Sec. II of this paper and nondimensionalized to simplify the analysis. A detailed treatment of the heat flow process is presented in Sec. III to derive expressions for the time when phase change ceases and the final widths of crystalline marks. The kinetics of the phase-change process are incorporated in Secs. IV and V to study the requirements for the initial peak temperature, and hence source energy density, in the medium during high-speed crystallization. Using this information, expressions are derived for the final crystalline mark widths and tail lengths that determine the recording resolution of the storage medium. Finally, perturbation analyses are carried out in Sec.

[a]Electronic mail: m.m.aziz@ex.ac.uk.

VI to study the influence of heat release during crystallization on heat flow in the material during the fast kinetics phase.

The phase-change process considered here is the rapid crystallization from the amorphous initial phase and does not involve crystallization through melt-quench processes.[11] In this work, it is assumed that the thermal anisotropies of the amorphous and crystalline phases have negligible effect on the phase-change process and hence on resolution of crystalline marks. Hence only the thermal parameters of the amorphous phase will be used in this paper. This has been shown to be valid recently by the authors for the class of phase-change materials used in data storage[12] and confirmed here with emphasis on the influence of latent heat of crystallization during ultrafast annealing. Moreover, the analysis excludes the influence of thermal layers on heat flow in the phase-change medium since the focus here is on the intrinsic thermal and kinetic parameters of the active layer during ultrafast heating. The effects of heat sinking and sandwiching layers are discussed in detail elsewere,[9,13–15] and their effects may be included to extend the present work following the analytical treatment in Ref. 10. Finally, the treatment of kinetics here does not take into account incubation times for the onset of crystallization.[5] Hence it applies more to melt-quenched or primed amorphous phase-change media.[16]

II. HEAT FLOW AND REACTION RATE EQUATIONS

The time dependent, isotropic heat conduction equation in one dimension is given by

$$\rho C_p \frac{\partial T(x,t)}{\partial t} = K \frac{\partial^2 T(x,t)}{\partial x^2}, \tag{1}$$

where T is the absolute temperature and ρ is the density of the material with thermal conductivity K and specific heat C_p. There is a small volume change associated with the phase-change process[6,17] ($\sim$6% for $Ge_2Sb_2Te_5$) and for simplicity ρ in Eq. (1) represents the average density of the amorphous and crystalline phases.

The rate of change in crystalline volume fraction, $\chi(x,t)$, will be described by the first-order, Arrhenius-type relationship:[18]

$$\frac{\partial \chi(x,t)}{\partial t} = [1-\chi(x,t)]A_c \exp\left[\frac{-E_c}{kT(x,t)}\right], \tag{2}$$

where E_c is the activation energy for crystallization and A_c is the frequency term; both are considered to be temperature independent. k is Boltzmann's constant and T is the absolute temperature. Since the onset time for the creation of critical nuclei or incubation time is not considered in Eq. (2), then the activation energy used would most likely be that for grain growth. Details of the assumptions involved and the derivation of the reaction rate equation in Eq. (2) were detailed by Avrami.[19–21]

The heat conduction and rate equations can be nondimensionalized to reduce the mathematical complexity of the analysis using the scaling relationships $x=x_o\eta$, $t=t_o\tau$, and $T(x,t)-T_o=T_o\psi(\eta,\tau)$, where x_o and t_o are the size scales of the variables in the system and T_o is the ambient temperature. The volume fraction of the crystalline material χ does not require rescaling. Substituting the rescaled variables and setting $Kt_o/(x_o^2C_p\rho)=1$ results in the nondimensionalized form of the heat equation:

$$\frac{\partial \psi(\eta,\tau)}{\partial \tau} = \frac{\partial^2 \psi(\eta,\tau)}{\partial \eta^2}. \tag{3}$$

Substituting the scaling relationships into Eq. (2) results in the nondimensionalized form of the kinetics equation

$$\frac{\partial \chi(\eta,\tau)}{\partial \tau} = [1-\chi(\eta,\tau)]\Delta \exp\left[\frac{-\gamma}{\psi(\eta,\tau)+1}\right], \tag{4}$$

where $\Delta=t_oA_c$ and $\gamma=E_c/(kT_o)$.

A. The heating source

Sources of heat energy such as lasers or probes in data storage applications typically produce symmetrical, bell-shaped temperature fields in the phase-change medium with tails that tend to the ambient temperature away from the center of the heat source. The Gaussian function conforms to this description and is used here as the initial temperature profile in the phase-change medium, written in normalized form as

$$\psi(\eta,0) = \psi_p e^{(-x_o^2/2\sigma^2)\eta^2}. \tag{5}$$

The parameter σ describes the width of this distribution at $e^{-1/2}$ or 0.6 of its peak value, $\psi_p=(T_p-T_o)/T_o$, with T_p being the initial peak temperature. The peak temperature in the medium reflects the magnitude of the power supplied by sources such as lasers in optical storage and voltages in probe systems and is an important control parameter particularly during ultrafast heating as will be discussed later.

The heat flow system described by Eq. (3) and the initial Gaussian profile is equivalent to a heat flow problem with an added heat generation term described by a Gaussian spatial function with a Dirac delta temporal profile, simulating an ultrafast heating pulse supplied by the heating source to the medium. This case is of practical importance in the study of the formation and resolution of recorded marks in ultrafast annealing regimes. The peak energy per unit volume of the medium, g_p, is then related to the peak temperature through

$$g_p = \frac{K}{\alpha}(T_p - T_o), \tag{6}$$

where $\alpha=K/\rho C_p$ is the thermal diffusivity of the medium. In the following analysis, the attention will be on the peak temperature as the main parameter rather than energy density. This is to enable direct comparison with characteristic temperatures in the system such as the melting temperature of the phase-change material. Equation (6) can be used when needed to calculate the corresponding energy density in the medium for the specific heating source.

III. ESTIMATION OF THE FINAL WIDTH OF THE CRYSTALLINE REGION WHEN PHASE CHANGE HAS CEASED

The amorphous-to-crystalline phase transition process is taken here to be thermally activated, and hence the spreading of the crystalline mark follows the heat diffusion in the material starting from the initial temperature profile. This transformation will take place within a region defined by the thermal profile in the medium where the temperature exceeds the crystallization temperature T_c of the phase-change medium. As heat diffuses through the material, the temperature continues to decrease until it falls below the T_c and phase change ceases. Therefore the final crystalline mark width is determined when thermal spreading, identified by the increase in the thermal contour $T=T_c$ (or $\psi=\psi_c$ in normalized form), stops.

For the Gaussian initial temperature profile, it can be shown that the solution to the isotropic heat flow problem in Eq. (3) is given by

$$\Psi(\eta,\tau)=\frac{\Psi_p e^{[-x_o^2/(2\sigma^2)/(1+2x_o^2\tau/\sigma^2)]\eta^2}}{\sqrt{1+2x_o^2\tau/\sigma^2}}. \tag{7}$$

The spatial location η_c at which $\psi=\psi_c$ where phase change ceases and defines the boundaries of the crystalline mark can be obtained from Eq. (7) and is given by

$$\eta_c=\pm\sqrt{\frac{-(1+2x_o^2\tau/\sigma^2)}{x_o^2/(2\sigma^2)}\ln\left(\frac{\Psi_c}{\Psi_p}\sqrt{1+\frac{2x_o^2}{\sigma^2}\tau}\right)}. \tag{8}$$

The isotherm at η_c will start to increase as heat diffuses from the initial temperature profile, reaches a maximum, and then decreases as temperature continues to fall and the spreading stops. Hence the time τ_c at which the boundary η_c is a maximum can be used as a realistic indicator of the end of thermal and hence amorphous-to-crystalline phase-change spreading. Thus maximizing Eq. (8) and solving for the normalized time yields

$$\tau_c=\frac{\sigma^2}{2x_o^2}\left[\frac{1}{e}\left(\frac{\Psi_p}{\Psi_c}\right)^2-1\right]. \tag{9}$$

Substituting Eq. (9) back into Eq. (8) yields the spatial distance, from the origin, over which spreading stops:

$$\eta_c^{\tau_c}=\pm\frac{\sigma}{x_o\sqrt{e}}\frac{\Psi_p}{\Psi_c}. \tag{10}$$

The width of the final crystalline mark, W, is then $W/x_o=2\eta_c^{\tau_c}$, or in dimensional form:

$$W=\frac{2\sigma}{\sqrt{e}}\frac{(T_p-T_o)}{(T_c-T_o)}. \tag{11}$$

The spatial locations where $T<T_c$ will also have a finite volume crystalline fraction and these define the tail regions of the final crystalline mark. The extent of these tails will be determined later in this paper. Equation (10) shows that the size of the recorded crystalline mark can be minimized by reducing the width of the initial temperature profile σ and by reducing the peak temperature Ψ_p, which should be sufficiently greater than T_c but less than the melting temperature T_m of the phase-change medium. The dependence of the peak temperature on the kinetic and thermal parameters of the material, which influences the mark size as indicated in Eq. (10), will be addressed next.

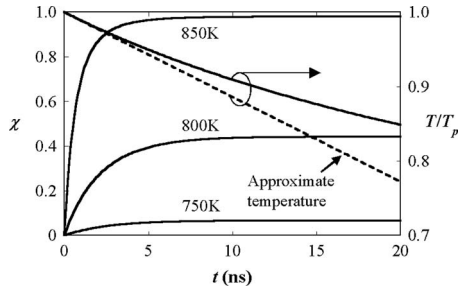

FIG. 1. Evolution of crystalline fraction with time at the location $x=0$ for different initial peak temperatures T_p. Also shown is the normalized peak temperature at the same location and its linear approximation.

IV. PEAK TEMPERATURE REQUIREMENT

So far, the choice of the initial peak temperature T_p in the medium, produced by the heating source, has been restricted only by the implicit requirement that it should be greater than the crystallization temperature T_c and less than the melting temperature T_m. In ultrafast heating, crystallization occurs during cooling rather than heating, and this puts more emphasis on the initial peak temperature as it determines the magnitude and rate of crystallization that can be achieved during cooling.

To achieve fast crystallization and hence obtain a sufficient level of crystalline fraction during cooling, the logical requirement would be for the crystallization rate to be higher than the cooling rate of the temperature in the medium, or

$$\left|\frac{\partial\chi}{\partial\tau}\right|>\left|\frac{\partial\Psi}{\partial\tau}\right|. \tag{12}$$

This requirement will be evaluated at the location of peak temperature, where $\eta=0$, as a representative location for the region where approximately uniform crystallization occurs (i.e., where $T>T_c$), within the time scale of thermal and phase-change spreading. After application of the initial temperature profile, it is expected that the crystallization rate is large and hence the fraction of crystalline material settles to the steady-state value within a short time. At these small times, the reduction in temperature with time may be represented by the linear approximation shown as the dashed line in Fig. 1, obtained by expanding Eq. (7) to first order:

$$\Psi(0,\tau)\approx\Psi_p\left(1-\frac{x_o^2}{\sigma^2}\tau\right), \tag{13}$$

with cooling rate $-\Psi_p x_o^2/\sigma^2$ [or $-\alpha(T_p-T_o)/\sigma^2$ in dimensional form]. Substituting Eq. (13) into Eq. (4) and integrating yields the evolution of volume fraction of crystalline material with time during the linear decrease in temperature at $\eta=0$ as

TABLE I. List of thermal, kinetic, and structural parameters for $Ge_2Sb_2Te_5$ available from literature for the amorphous phase. ρ is the density of the material, T_m and T_c are the melting and crystallization temperatures, respectively, C_p and K are the specific heat and thermal conductivity, respectively, L_c is the specific latent heat of crystallization, and α is the thermal diffusivity. E_c is the activation energy for crystallization and A_c is the frequency term.

Symbol	Value	Units
ρ	5995[a]	kg/m^3
T_m (5 K/min)	894[b]	K
T_c (80 K/min)	446[b]	K
C_p	218[c]	J/kg K
L_c	3.8[d]	kJ/kg
K (300 K)	0.23[e,f]	W/m K
$\alpha=K/(\rho C_p)$	176×10^{-9}	m^2/s
E_c	2.2[g,h]	eV
A_c	1.5×10^{22} [h]	s^{-1}

[a]Average density of amorphous and crystalline phases, Refs. 6 and 17.
[b]Reference 22.
[c]Dulong–Petit value for the molar heat capacity at constant pressure, i.e., $C=3Nk$ for nine atoms of $Ge_2Sb_2Te_5$. Also appeared in Refs. 1 and 2.
[d]Reference 23.
[e]Reference 24.
[f]Reference 25.
[g]Reference 26.
[h]Reference 5.

$$\chi(0,\tau)=1-[1-\chi(0,0)]\exp\left\{\frac{\Delta}{\Psi_p x_o^2/\sigma^2}\left[(\Psi_p+1-\Psi_p x_o^2\tau/\sigma^2)\times e^{-\gamma/(\Psi_p+1-\Psi_p x_o^2\tau/\sigma^2)}+\gamma\,\mathrm{Ei}\left(\frac{-\gamma}{\Psi_p+1-\Psi_p x_o^2\tau/\sigma^2}\right)-(\Psi_p+1)e^{-\gamma/(\Psi_p+1)}-\gamma\,\mathrm{Ei}\left(\frac{-\gamma}{\Psi_p+1}\right)\right]\right\}, \tag{14}$$

where $\chi(0,0)$ is the initial volume fraction of crystalline material and $\mathrm{Ei}(\cdot)$ is the exponential integral. Expanding Eq. (14) for small τ yields the linear approximation

$$1-\chi(0,\tau)\approx[1-\chi(0,0)][1-\Delta\tau e^{-\gamma/(\Psi_p+1)}]. \tag{15}$$

Differentiating Eqs. (13) and (15) and substituting into Eq. (12) lead to the first requirement for the initial peak temperature to ensure high crystallization rates:

$$\Psi_p+1>\left|\frac{\gamma}{\ln\{\Delta\sigma^2[1-\chi(0,0)]/x_o^2\}}\right|. \tag{16}$$

In deriving Eq. (16) use was made of the fact that $\gamma/(\Psi_p+1)>\ln(\Psi_p)$ since $\Psi_p\approx0\rightarrow3$ (i.e., T_P varies approximately in the range $T_o\rightarrow4T_o$) and $\gamma>1$. In dimensional form, Eq. (16) is

$$T_p>\left|\frac{E_c}{k\ln\{A_c\sigma^2[1-\chi(0,0)]/\alpha\}}\right|. \tag{17}$$

Equation (17) gives the minimum value of the initial peak temperature, and hence minimum source energy density from Eq. (6), that is needed in order to achieve a crystallization rate higher than the cooling rate in the medium and hence produce amorphous-to-crystalline phase change during cooling. Substituting the parameters in Table I, which are for a typical phase-change material employed in data storage systems, into Eq. (17) for the amorphous starting phase $[\chi(0,0)=0]$ produces $T_p>742$ K to satisfy the inequality in Eq. (12).

In addition to facilitating high crystallization rates, the magnitude of the initial peak temperature should also permit the production of adequate levels of crystalline volume fraction in the material during cooling to provide sufficient contrast for detection and readback. Figure 1 shows a plot of the fraction of crystalline material computed using Eq. (14) for different values of peak temperature when $\chi(0,0)=0$ (i.e., amorphous starting phase). This figure shows that a narrow temperature range above 800 K (approaching the melting temperature of the phase-change material considered here) is needed to produce acceptable volume fractions of crystalline material of 0.5 and above. It can also be seen in Fig. 1 that increasing the peak temperature increases the crystallization rate and reduces the crystallization time constant [time where the small time asymptote of the crystalline fraction given in Eq. (15) intersects the steady-state asymptote given by Eq. (18)]. In general, Fig. 1 shows approximately a 10 ns time scale for the amorphous-to-crystalline phase transition using the material parameters and one-dimensional geometry considered here. This time lies within the range where the linear approximation for the temperature in Eq. (13) is valid and is also in good agreement with picosecond, laser annealing crystallization experiments on phase-change media.[9]

Thus, in addition to satisfying the high crystallization rate requirement in Eq. (12), the magnitude of the peak temperature must also be controlled to produce sufficient levels of crystalline fraction (>0.5 here) for use in data storage applications. The final or steady-state value of crystalline fraction χ_s occurs in Eq. (14) when $\Psi_p+1\approx\Psi_p x_o^2\tau/\sigma^2$ and can be approximated using $1+e^{\zeta}\,\mathrm{Ei}(-\zeta)\approx1/(1+\zeta)$ and for large values of γ to

$$1-\chi_s\cong[1-\chi(0,0)]\exp\left[\frac{-\Delta\sigma^2}{x_o^2\gamma\Psi_p}(\Psi_p+1)^2e^{-\gamma/(\Psi_p+1)}\right]. \tag{18}$$

Equation (18) cannot be solved exactly for the peak temperature Ψ_p, but for typical values of Ψ_p in the range $0\rightarrow3$, the following good approximation is obtained:

$$\Psi_p+1\cong\frac{-\gamma}{\ln\left\{\frac{-\gamma x_o^2}{4\Delta\sigma^2}\ln\left[\frac{1-\chi_s}{1-\chi(0,0)}\right]\right\}}, \tag{19}$$

or in dimensional form:

$$T_p\cong\frac{-E_c}{k\ln\left\{\frac{-\alpha}{4A_c\sigma^2}\frac{E_c}{kT_o}\ln\left[\frac{1-\chi_s}{1-\chi(0,0)}\right]\right\}}. \tag{20}$$

The larger of Eqs. (17) and (20) can be used to determine the appropriate value of T_p to achieve high crystallization rates and sufficient level crystalline fraction χ_s during rapid annealing of phase-change media. For the material parameters listed in Table I, a value of $T_p=850$ K would sat-

TABLE II. List of phase-change materials used in data storage, their activation energies E_c, and their melting temperatures T_m from literature. Their peak temperatures T_p were calculated according to Eqs. (17) and (20) and the thermal parameters in Table I to achieve a final fraction of crystalline material of 0.9.

Material	E_c (eV)	T_p (K)	T_m (K)
$Ge_2Sb_2Te_5$	2.24[a]	850	894[b]
AgInSbTe	3.03[c]	1164	810[b]
$Ge_4Sb_1Te_5$	3.48[d]	1343	967[b]

[a]References 5 and 26.
[b]Reference 22.
[c]Reference 28.
[d]Reference 29.

isfy Eqs. (17) and (20) and yield a volume fraction of crystalline material of 0.9 and hence is used throughout this work.

The analytical expressions for the peak temperature in Eqs. (17) and (20) show that the peak temperature is directly proportional to the activation energy of crystallization. The effect of thermal diffusivity on peak temperature in these equations is of less significance because of the logarithmic dependence. The peak temperatures needed to satisfy the requirements in Eqs. (17) and (20) also occur within a narrow range that approaches the melting temperature of the phase-change medium under consideration, even for modest crystalline fractions χ_s. This could explain the published results of fast laser heating experiments of amorphous phase-change material which either lead to melting[9,27] or resulted in burned-out holes in the amorphous material.[8] Table II shows calculations of peak temperatures for a number of phase-change materials used in data storage using Eqs. (17) and (20) and using the representative thermal parameters in Table I for an initial Gaussian temperature profile with width $\sigma = 100$ nm. It can be seen from Table II that, for compositions other than $Ge_2Sb_2Te_5$, the required peak temperatures exceed the published melting temperatures for the respective materials. The theory produced here suggests the use of a material with low activation energy in order to reduce the peak temperature and avoid melting. Reducing the activation energy also has the effect of increasing the crystallization rate of the material, producing higher fractions of crystalline material, $\chi \sim 1$, at very short time scales. Even for a material such as $Ge_2Sb_2Te_5$, it would still be difficult to precisely control the energy of the heating source to achieve a peak temperature of 850 K, which is close to the melting temperature, in the medium. Thus in addition to controlling the peak temperature in the medium in this case, it would also be necessary to make use of buffer and heat sinking layers with the appropriate thermal diffusivity in the material stack to alleviate the stringent peak temperature requirement for fast crystallization in the phase-change layer.[9]

V. CRYSTALLINE MARK RESOLUTION

The width of the crystalline mark determines the possible linear and areal density in a storage medium. An important parameter that affects these densities is the extent of the tail regions of the crystalline mark where the volume fraction of crystalline material decreases from approximately 1 to 0. The extent of these tail regions determines how far crystalline bits can be written next to each other before they start to overlap and hence limits the linear density of the medium. It is therefore useful to obtain an estimate of the extent of these regions and their dependence on the material and recording parameters in the system.

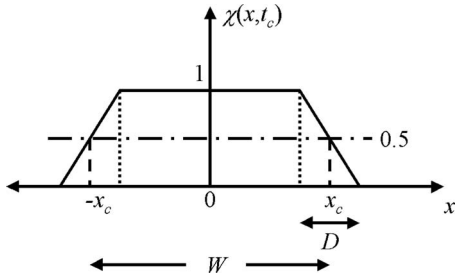

FIG. 2. Assumed spatial distribution of final crystalline mark after phase change is complete. For the $Ge_2Sb_2Te_5$ material parameters listed in Table I, theory showed $W=457$ nm and $D=24$ nm for an initial temperature pulse width $\sigma=100$ nm.

Previous work indicated that the transition or crystallization temperature T_c occurs when the reaction rate is maximum.[18,30] This condition can be applied at the location η_c (defining the crystalline-amorphous boundary of the final crystalline mark at time τ_c) to estimate the length of the tail regions. Hence maximizing Eq. (4) gives

$$\left.\frac{\partial \chi(\eta,\tau)}{\partial \eta}\right|_{\substack{\tau_c \\ \eta_c}} = \gamma \frac{[1-\chi(\eta_c,\tau_c)]}{(\Psi_c+1)^2} \times \left.\frac{\partial \Psi(\eta,\tau)}{\partial \eta}\right|_{\substack{\tau_c \\ \eta_c}}, \quad (21)$$

where the first term on the right-hand side of Eq. (21) represents the change in crystalline fraction with temperature $\partial\chi/\partial\Psi$. It will be taken here that the maximum reaction rate occurs within the transition region between the amorphous and crystalline phases where $\chi(\eta_c,\tau_c) \sim 0.5$ (natural transition point between a mark representing unity and a mark representing zero), implying that the spatial dependence of $\chi(\eta,\tau)$ over the tail region defined by D will have a sigmoid form. This is in line with theoretical work that showed that the fraction of crystallized material is approximately 0.63 at the maximum reaction rate[30] and that there is a finite spatial length for the amorphous-to-crystalline transition in the medium. Under typical operating conditions the onset temperature for the phase change (or temperature of maximum reaction rate) will not be orders of magnitude greater than room temperature; thus given that $\gamma \gg 1$ (~ 84 from Table I), Eq. (21) requires that $\left|\partial\chi(\eta,\tau)/\partial\eta\right|^{\tau_c}_{\eta_c} \gg \left|\partial\Psi(\eta,\tau)/\partial\eta\right|^{\tau_c}_{\eta_c}$. This clearly shows that the spatial gradient of the tail regions when phase change ceases is steeper than the spatial gradient of the temperature profile.

Assuming that the final crystalline mark at time τ_c has the profile shown in Fig. 2 where the tail regions are represented by a ramp function, then the slope of the ramp function at $\chi(\eta_c,\tau_c) \sim 0.5$ is

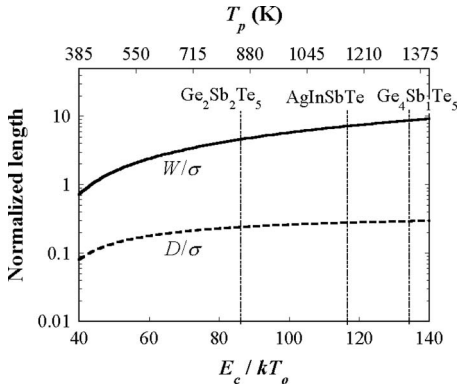

FIG. 3. Variation in crystalline mark width W and tail length D with activation energy. Also shown on the upper x axis is the calculated corresponding peak temperature. The thermal parameters listed in Table I were used in the calculations. This plot favors small activation energies (and hence reduced peak temperatures) to minimize the width and tail length of the recorded mark.

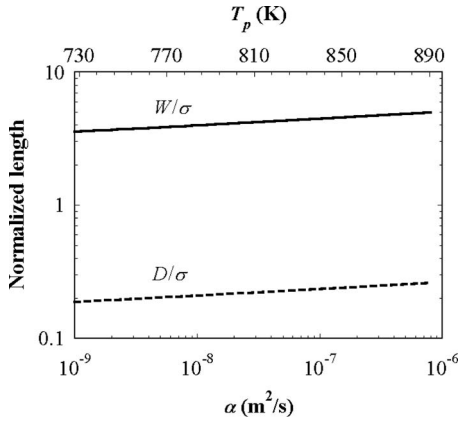

FIG. 4. Plot showing the dependence of final crystalline mark width W and tail length D on the thermal diffusivity of the medium. Also shown is the corresponding peak temperature for a fixed value of the activation energy E_c=2.2 eV.

$$\left| \frac{\partial \chi(\eta,\tau)}{\partial \eta} \right|_{\substack{\tau_c \\ \eta_c}} = \frac{x_o}{D}.$$

The spatial gradient of the temperature at η_c and τ_c from Eq. (7) is

$$\left| \frac{\partial \Psi(\eta,\tau)}{\partial \eta} \right|_{\substack{\tau_c \\ \eta_c}} = \sqrt{e}\frac{x_o}{\sigma}\frac{\Psi_c^2}{\Psi_p}.$$

Substituting the two spatial gradients in Eq. (21) and solving for D yields the tail length

$$D = \frac{2\sigma}{\sqrt{e}}\frac{\Psi_p}{\gamma}\left(\frac{1+\Psi_c}{\Psi_c}\right)^2 = \frac{2\sigma}{\sqrt{e}}\frac{k(T_p - T_o)}{E_c}\left(\frac{T_c}{T_c - T_o}\right)^2$$

$$= \frac{W}{(T_c - T_o)E_c/kT_c^2}, \tag{22}$$

where W is the width of the crystalline region given by Eq. (11). Equation (22) clearly shows that the tail length scales with the initial temperature distribution length σ and is inversely proportional to the activation energy of crystallization of the medium, in agreement with the results of the slope theory.[30] However, since the peak temperature is directly proportional to the activation energy from Eq. (20), the above dependence of the tail length changes in favor of small activation energies (and hence peak temperatures) to minimize the tail length.

Using a peak temperature of 850 K as determined previously, it is now possible to estimate the size of the final crystalline mark, including the tail lengths, after thermal and phase-change spreadings are complete. The final mark width W can be evaluated using Eq. (11) for an initial temperature pulse width σ=100 nm and is W=457 nm, while the tail length from Eq. (22) is D=24 nm. Hence the overall mark size $W+D$=481 nm.

Figure 3 shows the final computed crystalline mark widths and tail lengths as functions of the activation energy and the corresponding peak temperatures calculated using Eqs. (17) and (20) for the thermal parameters in Table I. It can be clearly seen from Fig. 3 that the width of the final crystalline marks, the tail length, and peak temperatures all decrease with reducing activation energy. Reducing the activation energy increases the crystallization rate, allowing the material to crystallize within very short time scales. Moreover, the resulting reduction in the operating peak temperature avoids melting and reduces the required energy supplied by heating sources.

The widths and tail lengths of final crystalline marks also exhibit a dependence on the thermal diffusivity of the medium through the peak temperature. This dependence is, however, logarithmic as can be observed from Eqs. (17) and (20) and therefore has less impact on the resolution of crystalline marks compared to the dependence on activation energy. Nevertheless, this dependence favors smaller thermal diffusivities to reduce the final crystalline mark width and tail length. The small thermal diffusivity reduces the cooling rate of the medium after the initial thermal profile, allowing sufficient time for the amorphous-to-crystalline transformation process to take place and to produce sufficient crystalline fractions before the temperature decreases significantly in the medium. Figure 4 shows that the final crystalline mark width W and tail length D increase only slightly for large increases in α due to the logarithmic dependence and that the change in peak temperature with increasing thermal diffusivity is also small.

Correlation moment analysis carried out by the authors to study the effect of thermal anisotropies during phase change,[12] which were based on the heat flow process alone, produced upper estimates for the time when phase change ceases and the time dependent correlation length of crystalline marks during the amorphous-to-crystalline phase transition process. The analytical work carried out in this paper takes into account the kinetics of the phase change and produced more practical times for when phase-change spreading stops and hence allows to compare the resolution of crystalline marks produced by this theory with that from the correlation moment analysis based on heat flow alone. Evaluating the correlation length $d_{\chi,\chi}(t_c)$ for the final crystalline mark profile in Fig. 2 using Eqs. (6) and (8) of Ref. 12 yields

$$d_{\chi,\chi}(t_c) = \sqrt{\frac{D^4 + 10D^2W^2 + 5W^4}{10(D^2 + 3W^2)}}. \tag{23}$$

Substituting the calculated values for W and D in Eq. (23) yields $d_{\chi,\chi}(t_c)=187$ nm. This value is smaller than the upper value estimated using correlation moment analysis (533 nm) for the same initial temperature profile and thermal parameters. This difference may be attributed to the overestimated time of the end of thermal spreading predicted using the correlation moment analysis which is equal to 350 ns, compared to 120 ns computed using Eq. (9) of this paper. This difference is expected since the upper estimators produced by the correlation moment analysis are based on the wider thermal profile in the medium rather than the actual and more confined profile of the crystalline mark which tends to follow a window function with sharp tails.

VI. EFFECT OF LATENT HEAT OF CRYSTALLIZATION

The authors recently reported that the influence of anisotropies in the thermal parameters of phase-change material used in data storage during the phase-change process is negligible.[12] This also applies to the effect of the release of latent heat during crystallization where the coefficient of the nonlinearity in the heat conduction equation due to latent heat, $\varepsilon = L_c/(C_p T_o)$, is small with values around 0.06 for phase-change materials used in storage applications such as $Ge_2Sb_2Te_5$, $Ge_4Sb_1Te_5$, and AgInSbTe.[22] As a result, the thermal anisotropies in this work were neglected, allowing the use of the simpler isotropic heat flow analysis. Nevertheless, it is constructive to understand the influence of latent heat of crystallization on the cooling rate and peak temperature requirements for different phase-change recording materials during ultrafast heating. Hence, first-order perturbation solutions for the nonlinear heat conduction equation and reaction rate equation, including the release of latent heat during crystallization, are derived in the Appendix.

The effect of latent heat is evident in Eq. (A13) which describes an increase in the dynamic temperature at $\eta=0$ due to an added, self-heating term after the application of a Gaussian temperature pulse. In particular, the cooling rate of the temperature at $\tau=0$ is now decreased from $-\Psi_p x_o^2/\sigma^2$ (the case with no latent heat where $\varepsilon=0$) to

$$\left.\frac{\partial \Psi}{\partial \tau}\right|_{\tau=0} = -\Psi_p \frac{x_o^2}{\sigma^2} + \varepsilon[1-\chi(0,0)]\Delta e^{-\gamma/(\Psi_p+1)} \tag{24}$$

due to the release of latent heat.

The consequence of the reduction in the cooling rate is less stringent requirements on the peak applied temperature (and hence energy density) in the phase-change material to achieve high crystallization rates and sufficient volume fractions of crystalline material during cooling. The high crystallization rate requirement in Eq. (12) can be evaluated again here to include the heat release during crystallization using Eq. (24) and by expanding Eq. (A14) to first order for small times to yield the same crystallization rate as for the unperturbed system as given by differentiating Eq. (15) with respect to τ. This results in the peak temperature requirement

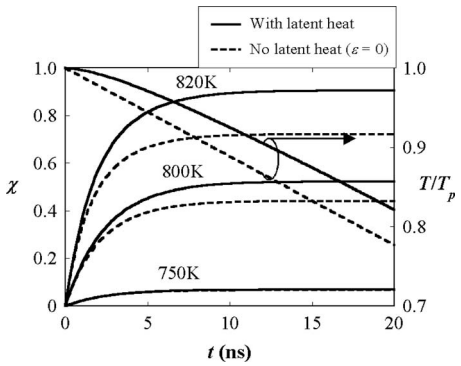

FIG. 5. Evolution of crystalline fraction with time at the location $x=0$ for different initial peak temperatures T_p with and without ($\varepsilon=0$) the effects of latent heat of crystallization. Also shown is the normalized peak temperatures at the same location and calculated for $T_p=820$ K. The latent heat reduces the cooling rate in the medium, thus increasing the volume fraction of crystalline material with modest reductions in peak temperature requirements.

$$T_p > \left| \frac{E_c}{k \ln\{A_c\sigma^2(1+\varepsilon)[1-\chi(0,0)]/\alpha\}} \right|, \tag{25}$$

which is similar to the inequality in Eq. (17) but now reduced by a factor of $\ln(1+\varepsilon)$ due to latent heat. The logarithmic dependence means that the release of latent heat has negligible effect on the crystallization rate. This can be seen by substituting the parameters in Table I into Eq. (25) yielding a $T_p > 740$ which represents a negligible reduction in temperature compared to the case where latent heat is neglected ($T_p > 742$).

The reduction in cooling rate due to the release of latent heat also allows the phase-change material to produce higher levels of crystalline volume fractions. This effect can be seen in Fig. 5 which shows volume fractions of crystalline material, computed using Eq. (A14), for different values of peak applied temperatures and compared with crystalline fractions with no added latent heat ($\varepsilon=0$). The increase in volume fraction with the release of latent heat can also be appreciated by determining the steady-state value of χ in Eq. (A14) which, using the same approximations used to derive Eq. (18), is now increased to

$$\chi_s \cong 1 - [1-\chi(0,0)]\exp\left[\frac{-4\Delta\sigma^2}{x_o^2\gamma} e^{-\gamma/(\Psi_p+1)}\right] \times \left\{1 - 2\varepsilon\frac{[1-\chi(0,0)]\Delta^2}{\gamma x_o^4/\sigma^4} e^{-2\gamma/(\Psi_p+1)}\right\}. \tag{26}$$

Equation (26) cannot be solved exactly for the peak temperature Ψ_p and was therefore determined numerically to achieve a steady-state volume fraction $\chi_s=0.9$. The peak temperature requirement in this case is $T_p \approx 820$ K, which again is a modest reduction compared to the requirement when latent heat was neglected in the previous analysis (850 K).

The perturbation analyses carried out in this paper are valid for small values ε and particularly at small times τ where the kinetics are important. Moreover, the theory was simplified to ignore the movement of the two phases in the material, and therefore cannot predict the propagation dynamics of the crystallization front, and hence the width of the

final crystalline mark when phase change ceases. This is more the domain of numerical analysis[31,32] which showed an increase in the velocity of the crystalline-amorphous front with the increase in latent heat during crystallization. This effect is expected to be small for the material parameters listed in Table I due to the small value of ε and would be significant for Sb-rich material having relatively large latent heat of crystallization with $L_c/C_p=333$ K (Ref. 31) (hence $\varepsilon>1$).

VII. CONCLUSIONS

An analytical study was presented that predicts the resolution of the final recorded crystalline marks during ultrahigh heating where the heating source has a Dirac delta function time profile and applicable to melt-quenched or primed amorphous media where there is no incubation time.

The analysis produced an expression for the time when thermal spreading stops as the time where the location at which $T=T_c$ is a maximum. Using this time, an expression for the width of the final crystalline mark was obtained that scales with the width of the initial temperature profile and proportional to the initial peak temperature. This expression emphasized the importance of the value of the peak initial temperature (and hence supplied heat energy) in determining the crystallization rate and final volume of crystalline fraction. Imposing the requirements that the crystallization rate be greater than the cooling rate after application of the initial temperature profile and that there exists a sufficient volume fraction of crystalline material ($\chi>0.5$) use in data storage applications, two closed-form expressions for the peak temperature were produced. These expressions can be used to determine the required peak temperature (and hence heating source energy density) as a function of the kinetic and thermal parameters of the phase-change material. These expressions showed explicitly that the peak temperature is directly proportional to the activation energy of crystallization and less significantly on the thermal diffusivity of the material. Using published parameters for $Ge_2Sb_2Te_5$ and other compositions that are used in data storage applications, the derived expressions revealed that the required initial peak temperatures were very close or exceeded the melting temperature of the material, which agrees with the published observations of fast laser heating experiments on phase-change media. Thus to reduce this peak temperature the theory suggests the use of phase-change material with lower activation energy to increase the crystallization rate and final volume fraction of crystalline material. In addition to this, the cooling rate of the material can be reduced, although to a lesser extent, by reducing the thermal diffusivity of the material.

By maximizing the reaction rate of crystallization at the location and time where phase change ceases, an analytical expression was developed that described the extent of the tail region in the final crystalline mark. It was found that the tail length decreased with decreasing activation energy (and hence peak temperature), which is desirable to increase the linear density of the storage medium.

Therefore to minimize the final crystalline mark width and its tail length, and hence increase the resolution of the phase-change medium during ultrafast crystallization, the theory presented in this paper showed that a material with low activation energy of crystallization and of low thermal diffusivity would be needed. This would reduce the required initial peak temperature to avoid melting, increase the crystallization rate, and achieve sufficient levels of crystallization in the material within a 10 ns time scale.

Perturbation analyses were also carried out to study the role of the release of latent heat during rapid crystallization. The analyses revealed a reduction in the cooling rate of the medium due to the release of latent heat which leads to the production of higher levels of crystalline volume fraction using lower peak temperatures. This effect, however, was found to be modest for the class of phase-change material used currently in data storage.

APPENDIX: PERTURBATION ANALYSIS OF HEAT FLOW EQUATION INCLUDING THE RELEASE OF LATENT HEAT DURING PHASE-CHAGE

Assuming that there are no anisotropies in the thermal parameter of the two phases in the material, that there is no motion of the phases, and that pressure is constant, the normalized heat conduction equation including the latent heat of crystallization is given by[12]

$$\frac{\partial\Psi(\eta,\tau)}{\partial\tau}=\frac{\partial^2\Psi(\eta,\tau)}{\partial\eta^2}+\varepsilon\frac{\partial\chi(\eta,\tau)}{\partial\tau}, \tag{A1}$$

where $\varepsilon=L_c/(C_pT_o)$ and χ is the volume fraction of crystalline material. Since $\varepsilon<1$, the solution to Eq. (A1) can be written as a first-order perturbation series in ε:

$$\Psi(\eta,\tau)=\Psi_0(\eta,\tau)+\varepsilon\Psi_1(\eta,\tau), \tag{A2}$$

where Ψ_0 and Ψ_1 are the linear and nonlinear (correction) temperatures, respectively, that need to be determined. Substituting Eq. (A2) into Eq. (A1) yields

$$\frac{\partial\Psi_0(\eta,\tau)}{\partial\tau}+\varepsilon\frac{\partial\Psi_1(\eta,\tau)}{\partial\tau}=\frac{\partial^2\Psi_0(\eta,\tau)}{\partial\eta^2}+\varepsilon\frac{\partial^2\Psi_1(\eta,\tau)}{\partial\eta^2}+\varepsilon\frac{\partial\chi(\eta,\tau)}{\partial\tau}. \tag{A3}$$

Substituting Eq. (A2) into the rate equation (2), expanding for small ε, and integrating yields the explicit solution

$$\chi(\eta,\tau)=1-[1-\chi(\eta,0)]\times\exp\left\{-\Delta\int_0^\tau\exp\left[\frac{-\gamma}{\Psi_0(\eta,\tau)+1}\right]d\tau'\right\}\times\left\{1-\varepsilon\Delta\gamma\int_0^\tau\exp\left[\frac{-\gamma}{\Psi_0(\eta,\tau)+1}\right]\times\left\{\frac{\Psi_1(\eta,\tau)}{[\Psi_0(\eta,\tau)+1]^2}\right\}d\tau'\right\}, \tag{A4}$$

where $\chi(\eta,0)$ is the volume fraction of crystalline material at time $\tau=0$. Hence the volume fraction of crystalline material can be written in the form of the series

$$\chi(\eta,\tau) = \chi_0(\eta,\tau) + \varepsilon\chi_1(\eta,\tau), \tag{A5}$$

where χ_0 is the solution of Eq. (A4) when $\varepsilon=0$ and χ_1 is the second term on the right-hand side of Eq. (A4).

Substituting Eq. (A5) into Eq. (A3) and matching terms up to first order in ε produces the two linear partial differential equations for Ψ_0 and Ψ_1:

$$\frac{\partial\Psi_0(\eta,\tau)}{\partial\tau} = \frac{\partial^2\Psi_0(\eta,\tau)}{\partial\eta^2}, \tag{A6}$$

$$\frac{\partial\Psi_1(\eta,\tau)}{\partial\tau} = \frac{\partial^2\Psi_1(\eta,\tau)}{\partial\eta^2} + \varepsilon\frac{\partial\chi_0(\eta,\tau)}{\partial\tau}, \tag{A7}$$

subject to the boundary conditions that $(\Psi_0,\Psi_1)\to 0$, $\forall\tau \geq 0$, and the initial conditions that $\Psi_0(\eta,0)=f(\eta)$ and $\Psi_1(\eta,0)=0$, where $f(\eta)$ is the Gaussian profile given by Eq. (5).

The solution of Eq. (A6) for Ψ_0 is given by Eq. (7). Expanding this solution for small τ for simplicity gives

$$\Psi_0(0,\tau) \approx \Psi_p e^{(-x_o^2/2\sigma^2)\eta^2}\left[1 - \frac{x_o^2}{\sigma^2}\tau\left(1 - \frac{x_o^2}{\sigma^2}\eta^2\right)\right]. \tag{A8}$$

The zeroth-order term for the volume of crystalline fraction, χ_0, can now be determined by substituting Eq. (A8) into the first term on the right-hand side of Eq. (A4). Integration yields the expression in Eq. (14) but with Ψ_p replaced by $\Psi_p e^{(-x_o^2/2\sigma^2)\eta^2}$ and x_o^2/σ^2 replaced by $x_o^2/\sigma^2(1-x_o^2\eta^2/\sigma^2)$. Again expanding to first order around $\tau=0$ for simplicity yields the linear approximation

$$1 - \chi_0(\eta,\tau) \approx [1-\chi(\eta,0)]\left\{1 - \exp\left[\frac{-\gamma}{\Psi_p e^{(-x_o^2/2\sigma^2)\eta^2}+1}\right]\tau\right\}. \tag{A9}$$

The temperature Ψ_1 due to latent heat can now be determined using the derivative of Eq. (A9) with respect to τ as the source term in Eq. (A7). To produce an analytical solution to Eq. (A7), the following good approximation was used for Eq. (A9):

$$1 - \chi_0(\eta,\tau) \approx [1-\chi(\eta,0)]\left[1 - \Delta\exp\left(\frac{-\gamma}{\Psi_p+1} - \lambda\eta^2\right)\tau\right], \tag{A10}$$

with $\lambda=(\gamma\Psi_p x_o^2/\sigma^2)/2(\Psi_p+1)^2$. Differentiating Eq. (A10) with respect to τ, substituting in Eq. (A7), and solving produces the closed-form solution for the correction temperature Ψ_1:

$$\Psi_1(\eta,\tau) = \frac{[1-\chi(\eta,0)]\Delta}{2\lambda}e^{-\gamma/(\Psi_p+1)} \times\left\{e^{-\lambda\eta^2/(1+4\lambda\tau)}\sqrt{1+4\lambda\tau} - e^{-\lambda\eta^2} - \eta\sqrt{\pi\lambda}\left[\mathrm{erf}(\eta\sqrt{\lambda}) - \mathrm{erf}\left(\frac{\eta\sqrt{\lambda}}{\sqrt{1+4\lambda\tau}}\right)\right]\right\}, \tag{A11}$$

where erf(·) is the error function.

Using Eqs. (A8) and (A11) into Eq. (A2) provides an approximate analytical solution for the dynamic temperature in the phase-change layer during crystallization after the application of an infinitely short Gaussian temperature pulse and including the effect of the release of latent heat. The corresponding crystalline volume fraction can now be evaluated by substituting Eqs. (A8) and (A11) into Eq. (A4).

The focus here is on the location of maximum temperature in the medium to represent an approximate region of uniform crystallization. In this case, the normalized temperature evaluated at $\eta=0$ from Eqs. (A8) and (A11) into Eq. (A2) becomes

$$\Psi(0,\tau) \approx \Psi_p\left(1 - \frac{x_o^2}{\sigma^2}\tau\right) + \varepsilon\frac{[1-\chi(0,0)]\Delta}{2\lambda}e^{-\gamma/(\Psi_p+1)} \times(\sqrt{1+4\lambda\tau}-1). \tag{A12}$$

To be able to derive an analytical expression for the volume fraction of crystalline material in Eq. (A4) at $\eta=0$, the square root in Ψ_1 can be expanded for small values of τ using a first-order Padé approximation. yielding

$$\Psi(0,\tau) \approx \Psi_p\left(1 - \frac{x_o^2}{\sigma^2}\tau\right) + \varepsilon[1 - \chi(0,0)]\Delta e^{-\gamma/(\Psi_p+1)}\frac{\tau}{1+\lambda\tau}, \tag{A13}$$

which upon substitution, along with Ψ_0 at $\eta=0$, into Eq. (A4) and integration gives

$$\chi(0,\tau) = \chi_0(0,\tau) + \varepsilon[1-\chi_0(0,\tau)]\frac{\gamma[1-\chi(0,0)]}{[\Psi_p x_o^2/\sigma^2 + \lambda(\Psi_p+1)]}\Delta^2 e^{-\gamma/(\Psi_p+1)} \times\left\{e^{-\gamma\lambda/[\Psi_p x_o^2/\sigma^2+\lambda(\Psi_p+1)]} \times\left\{\mathrm{Ei}\left[\frac{-\gamma\Psi_p x_o^2/\sigma^2}{(\Psi_p+1)(\Psi_p x_o^2/\sigma^2+\lambda(\Psi_p+1))}\right] - \mathrm{Ei}\left[\frac{-\gamma\lambda}{\Psi_p x_o^2/\sigma^2+\lambda(\Psi_p+1)} - \frac{\gamma}{(\Psi_p+1)-\Psi_p x_o^2\tau/\sigma^2}\right]\right\} - \frac{(\Psi_p+1)[\Psi_p x_o^2/\sigma^2+\lambda(\Psi_p+1)]}{\gamma\Psi_p x_o^2/\sigma^2}\{e^{-\gamma/[(\Psi_p+1)-\Psi_p x_o^2\tau/\sigma^2]} - e^{-\gamma/(\Psi_p+1)}\}\right\}, \tag{A14}$$

where $\chi_0(0,\tau)$ is given by Eq. (14).

The perturbation analysis carried out here is valid provided that the second term in the series expansion of Eq. (A12) [or Eq. (A13)] is smaller than the first term, i.e., ε is small. This also requires that the slope of the temperature remains approximately negative.

[1]C. Peng, L. Cheng, and M. Mansuripur, J. Appl. Phys. **82**, 4183 (1997).
[2]T. Ohta, K. Inoue, M. Uchida, K. Yoshioka, T. Akiyama, S. Furukawa, K. Nagata, and S. Nakamura, Jpn. J. Appl. Phys., Suppl. **28**, 123 (1989).
[3]C. D. Wright, M. Armand, and M. M. Aziz, IEEE Trans. Nanotechnol. **5**, 50 (2006).
[4]C. A. Volkert and M. Wuttig, J. Appl. Phys. **86**, 1808 (1999).
[5]V. Weidenhof, I. Friedrich, S. Ziegler, and M. Wuttig, J. Appl. Phys. **89**, 3168 (2001).
[6]O. Bichet, C. D. Wright, Y. Samson, and S. Gidon, J. Appl. Phys. **95**, 2360 (2004).
[7]N. Ohshima, J. Appl. Phys. **79**, 8357 (1996).
[8]K. Watabe, P. Polynkin, and M. Mansuripur, Appl. Opt. **43**, 4033 (2004).
[9]J. Siegel, A. Schropp, J. Solis, C. N. Afonso, and M. Wuttig, Appl. Phys. Lett. **84**, 2250 (2004).
[10]M. M. Aziz and C. D. Wright, J. Appl. Phys. **99**, 034301 (2006).
[11]J. Solis and C. N. Afonso, Appl. Phys. A: Mater. Sci. Process. **76**, 331 (2003).
[12]M. R. Belmont, M. M. Aziz, and C. D. Wright, J. Appl. Phys. **104**, 044901 (2008).
[13]G. Zhou, Mater. Sci. Eng., A **304–306**, 73 (2001).
[14]H. C. F. Martens, R. Vlutters, and J. C. Prangsma, J. Appl. Phys. **95**, 3977 (2004).
[15]N. Ohshima, J. Appl. Phys. **79**, 8357 (1996).
[16]P. K. Khulbe, E. M. Wright, and M. Mansuripur, J. Appl. Phys. **88**, 3926 (2000).
[17]T. Nonaka, G. Ohbayashi, Y. Toriumi, Y. Mori, and H. Hashimoto, Thin Solid Films **370**, 258 (2000).
[18]H. E. Kissinger, Anal. Chem. **29**, 1702 (1957).
[19]M. Avrami, J. Chem. Phys. **7**, 1103 (1939).
[20]M. Avrami, J. Chem. Phys. **8**, 212 (1940).
[21]M. Avrami, J. Chem. Phys. **9**, 177 (1941).
[22]J. Kalb, F. Spaepen, and M. Wuttig, J. Appl. Phys. **93**, 2389 (2003).
[23]A. Kalb, M. Wuttig, and F. Spaepen, J. Mater. Res. **22**, 748 (2007).
[24]E. Kim, S. Kwun, S. Lee, H. Seo, and J. Yoon, Appl. Phys. Lett. **76**, 3864 (2000).
[25]V. Giraud, J. Cluzel, V. Sousa, A. Jacquot, A. Dauscher, B. Lenoir, H. Scherrer, and S. Romer, J. Appl. Phys. **98**, 013520 (2005).
[26]I. Friedrich, V. Weidenhof, W. Njoroge, P. Franz, and M. Wuttig, J. Appl. Phys. **87**, 4130 (2000).
[27]K. Sokolowski-Tinten, J. Solis, J. Bialkowski, J. Siegel, C. N. Afonso, and D. von der Linde, Phys. Rev. Lett. **81**, 3679 (1998).
[28]W. K. Njoroge and M. Wuttig, J. Appl. Phys. **90**, 3816 (2001).
[29]D. Wamwangi, W. Njoroge, and M. Wutting, Thin Solid Films **408**, 310 (2002).
[30]M. M. Aziz and C. D. Wright, J. Appl. Phys. **97**, 103537 (2005).
[31]D. A. Kurtze, W. Saarloos, and J. D. Weeks, Phys. Rev. B **30**, 1398 (1984).
[32]M. Okuda, H. Inaba, and S. Usuda, Proceedings of the European\Phase Change and Ovonics Symposium E\PCOS03, 2003 (unpublished).